Nonlinear climate response to regional brightening of tropical marine stratocumulus

Spencer Hill[1] and Yi Ming[2]

Received 20 April 2012; revised 3 July 2012; accepted 8 July 2012; published 14 August 2012.

[1] To counteract global warming, there have been suggestions to increase the albedo of low-level marine clouds through the aerosol indirect effects by injecting them with sea salt. However, the full climate response to this geoengineering scheme is currently poorly understood. We simulate cloud seeding in a coupled mixed-layer ocean-atmosphere general circulation model in order to identify the specific physical mechanisms through which seeding could perturb the climate system's radiative balance, and cause temperature and precipitation changes. Seeding stratocumulus decks over three tropical maritime regions in the North Pacific, South Pacific and South Atlantic produces strong local reductions in solar absorption. Over half of the radiative cooling is due to direct scattering of solar radiation by the added sea salt aerosols, while the rest comes from enhancement of the local cloud albedo. The oceanic cooling due to the seeding over the southeastern equatorial Pacific induces a La Niña-like response, with tropical precipitation changes resembling La Niña anomalies and teleconnections occurring in the mid-latitude North Pacific and North America. Additionally, model runs in which only one of the three regions is seeded indicate nonlinearity in the climate response. We identify dynamical and thermodynamical constraints respectively on the temperature and hydrological cycle responses to cloud seeding, but the full response to such geoengineering remains poorly constrained. **Citation:** Hill, S., and Y. Ming (2012), Nonlinear climate response to regional brightening of tropical marine stratocumulus, *Geophys. Res. Lett.*, *39*, L15707, doi:10.1029/2012GL052064.

1. Introduction

[2] Enhancing the albedo and lifetime of marine boundary layer clouds by injecting them with sea salt aerosols has previously been proposed as a geoengineering method of mitigating global warming [*Latham*, 1990, 2002]. The added aerosols would act as cloud condensation nuclei, thereby inducing local cooling through the aerosol first (cloud albedo) [*Twomey*, 1977] and second (cloud lifetime) [*Albrecht*, 1989] indirect effects. Initial model studies have suggested that such a cloud seeding scheme could brighten marine stratocumulus [*Latham et al.*, 2008], offsetting a significant fraction of the projected global warming [*Latham et al.*, 2008; *Jones et al.*, 2009; *Rasch et al.*, 2009]. This must be taken in context, however, that the aerosol indirect effects are poorly understood [e.g., *Lohmann et al.*, 2010].

[3] Cloud seeding could alter regional precipitation patterns vital to human society and/or ecosystems. Given the difficulty of accurately resolving precipitation on these scales in current generation coarse-resolution climate models, constraining these unintended consequences therefore requires a solid theoretical understanding of not only cloud seeding itself but also general cloud processes key to determining the climate response to a forcing.

[4] However, study of the climate response to cloud seeding has only just begun. Using a coupled atmosphere-ocean GCM (AOGCM) [*Jones et al.*, 2009, hereinafter J09] increased cloud droplet number concentration (N_d) to 375 cm^{-3} over three tropical regions (Figure 1 of J09) in addition to A1B emissions scenario greenhouse gas forcing. *Rasch et al.* [2009, hereinafter R09] imposed doubled CO_2 forcing (710 ppmv CO_2) and increased N_d to 1000 cm^{-3} between 850 and 1000 hPa over fixed percentages of the ocean surface (20, 30, 40, or 70% of total ocean area) in a series of AOGCM experiments, with seeding locations varying in time according to the location of the most susceptible clouds.

[5] In the present study, we use an atmosphere general circulation model (AGCM) coupled to a mixed-layer ocean model to simulate the impacts of cloud seeding on radiation, surface temperature (T) and precipitation (P). We also explore the linearity of the climate response to cloud seeding by comparing simulations with different geographical seeding areas.

2. Methodology

[6] We use a version of the Geophysical Fluid Dynamics Laboratory (GFDL) AM2.1 AGCM [*GFDL Global Atmospheric Model Development Team*, 2004] to evaluate the top-of-atmosphere (TOA) radiative imbalances caused by cloud seeding. This version features a prognostic scheme of N_d that allows for explicit consideration of the size distributions and chemical compositions of multiple aerosol types including sea salt [*Ming et al.*, 2006, 2007], enabling simulation of both the first and second aerosol indirect effects. The AGCM runs are for 17 model years with the first year as spin-up, and are used solely for evaluating the forcing. We then couple the AGCM to a mixed-layer ocean model to simulate the resulting equilibrium climate response. A detailed description of the coupled model configuration can be found in *Ming and Ramaswamy* [2009]. Results are averaged over the last 20 years of the 80-year coupled mixed-layer ocean-AGCM simulation. In order to discern the forced signal forced from the model's natural variability, we apply Student's t test at the 95% confidence level.

[1]Program in Atmospheric and Oceanic Sciences, Princeton University, Princeton, New Jersey, USA.
[2]Geophysical Fluid Dynamics Laboratory, NOAA, Princeton, New Jersey, USA.

Corresponding author: S. Hill, Program in Atmospheric and Oceanic Sciences, Princeton University, Princeton, NJ 08540, USA. (spencerh@princeton.edu)

0094-8276/12/2012GL052064

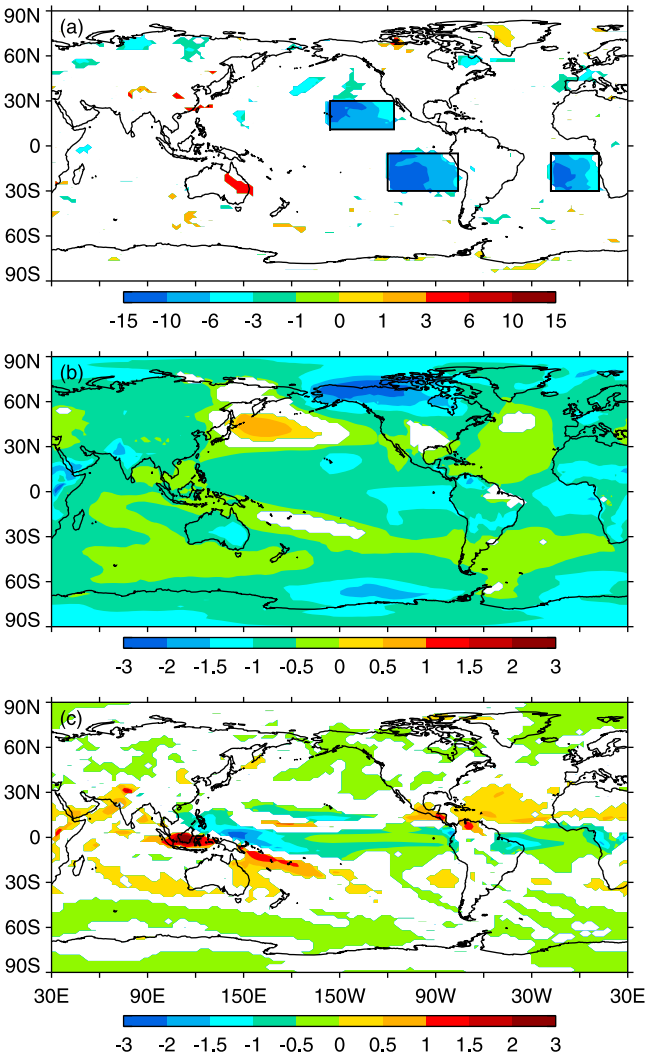

Figure 1. Annual-mean changes in (a) radiative flux perturbation (W m^{-2}), (b) surface temperature (K), and (c) precipitation (mm day^{-1}) in ALL. Areas shaded white are not statistically significant at the 95% confidence level.

[7] We simulate cloud seeding by increasing sea salt aerosol concentrations fivefold for all size bins below the 850 hPa level within three regions located in the tropical North Pacific (NP), South Pacific (SP), and South Atlantic (SA) (boxed regions in Figure 1a). These climatological subsidence regions feature persistent low clouds and, being remote from anthropogenic aerosol sources, usually have lower aerosol burdens and N_d than continental or polluted ocean regions. Since cloud albedo change scales better with fractional N_d change than absolute change, these regions have been identified previously as being susceptible to seeding [*Latham et al.*, 2008]. The locations of the regions follow those in J09 (Figure 1 of J09), though ours cover nearly twice as much area (Table 1). The somewhat *ad hoc* choice of a fivefold increase makes the magnitude of the resulting forcing comparable to that of greenhouse gases. In addition to one non-seeded control run (CONT) and one run in which all three regions are seeded (ALL), there are three individual region runs in which only one of the regions is seeded (NP, SP, and SA).

[8] To isolate the impacts of cloud seeding on climate, we keep fixed the levels of greenhouse gases and aerosol species (other than the aforementioned changes to sea salt) at pre-industrial (PI) levels. Analysis of the combined response to both cloud seeding and anthropogenic emissions will be addressed in a future study.

3. Results

3.1. Radiative Flux Perturbation

[9] We quantify changes to the radiative budget in terms of radiative flux perturbation (RFP) [*Haywood et al.*, 2009]. That is, in the AGCM-only runs we allow the atmosphere and land to respond to the injected aerosols while keeping sea surface temperatures (SST) fixed, and then take the TOA radiative flux difference between perturbation and control runs. RFP has been shown to be a good predictor of the resulting change in T [*Hansen et al.*, 2007; *Ming et al.*, 2010; *Persad et al.*, 2012] and is a plausible way to quantify the aerosol indirect effects [*Lohmann et al.*, 2010]. We note that "regressed radiative forcing" has been used as an alternative to RFP [*Gregory et al.*, 2004; *Ban-Weiss et al.*, 2011].

[10] The fivefold in-situ increase of sea salt aerosols produces strong reductions in solar absorption locally. The mean in-region RFP – that is, RFP averaged over the seeded areas only – is -8.5 W m^{-2} in ALL, and the global-mean is -0.73 W m^{-2}. The mean RFP over non-seeded areas is -0.20 W m^{-2}, which is deemed statistically insignificant as it is within the 95% confidence interval of the model's natural variation (0 ± 0.23 W m^{-2}). This indicates that the

Table 1. Surface Area for Each Seeding Region (% of the Total Earth Surface Area), Mean Fractional Change in N_d Within the Seeding Region(a) Between 850–1000 hPa, Mean RFP Within the Seeding Region(s) (W m^{-2}), Global-Mean RFP (W m^{-2}), Global-Mean δT (K), and Climate Sensitivity λ (K m^2 W^{-1})[a]

Run	Area (%)	$\delta N_d/N_d$	In-Region RFP (W m^{-2})	Global-Mean RFP (W m^{-2})	δT (K)	λ (K W^{-1} m^{-2})
ALL	6.4	2.1	−8.5	−0.73	−0.53	0.73
NP	1.9	2.5	−8.8	−0.36	−0.15	0.42
SP	2.6	2.1	−8.8	−0.41	−0.42	1.02
SA	1.8	1.9	−7.2	−0.31	−0.06	0.19
SUM	6.4	2.1	−8.5	−0.73	−0.63	0.86
J09 ALL	3.3		−32.1	−0.97	−1.78	1.83
J09 SP	1.5		−30.0	−0.52	−0.78	2.27
R09 20%	14.2				−0.94	
R09 70%	50.4				−2.15	

[a]ALL and SUM are identical in all categories other than δT and λ. Note that one should use caution in comparing the three studies as they differ in experimental design; see text, J09, and R09 for details.

radiative effects of cloud seeding are mostly confined locally.

[11] Decomposing RFP into clear- and cloudy-sky components further elucidates the radiative impacts. Clear-sky RFP captures direct scattering, while cloudy-sky RFP measures the aerosol indirect effects (note that this would not hold if the aerosols were absorbing instead of scattering [see *Persad et al.*, 2012]). Global-mean clear- and cloudy-sky RFP in ALL are -0.41 and -0.32 W m^{-2}, respectively. Thus, over half of the radiative effect comes from direct scattering, a larger fraction than that found by *Partanen et al.* [2012]. This is significant given that, by specifying N_d directly, prior response studies such as J09 and R09 do not capture direct scattering. The remaining RFP stems from the injected aerosols' microphysical effect on clouds. Averaged over all three seeding regions, N_d increases by 2.1 times over its control values, from 69 cm^{-3} in CONT to 148 cm^{-3} at the levels between 850–925 hPa (Table 1).

[12] In each region, RFP is weakest nearest neighboring continental landmasses (Figure 1a) due to two factors. First, like many others, this AGCM under-represents marine stratocumulus decks near land on the grid scale [*GFDL Global Atmospheric Model Development Team*, 2004]. As such, cloudy-sky RFP and thus all-sky RFP are likely underestimated. Second, higher baseline aerosol concentrations near land cause N_d to be higher there in CONT. Thus, the fractional increase in N_d (and therefore absolute increase in cloud albedo) is less than in cleaner conditions farther out to sea.

3.2. Changes in Temperature

[13] We now consider the response of the coupled mixed-layer ocean-AGCM to the RFP, beginning with T. The spatial distribution of T changes in ALL is much smoother than that of the highly localized RFP (Figure 1b). Because the Coriolis parameter is small near the equator, the tropical free troposphere (FT) cannot sustain strong horizontal temperature gradients [e.g., *Sobel et al.*, 2001; *Kang et al.*, 2009]. The tight convective coupling between the tropical surface and free troposphere extends this dynamical constraint to the surface (albeit to a lesser extent than in the free troposphere). Thus, cooling beneath the brightened clouds necessarily gets re-distributed through the whole tropics. Cooling also extends to the mid- and high-latitudes, except for warming over the mid-latitude North Pacific discussed below.

[14] In this study, the initially steady state climate is subjected to a stepwise forcing, analogous to an instant doubling of CO_2; the system then continuously adjusts to a new steady state. The climate sensitivity (λ) is defined as the difference in global-mean T between the initial and new climate states (latter minus former) normalized by the forcing (measured in RFP). Global-mean temperature change (δT) from CONT to ALL is -0.53 K, resulting in a λ of 0.72 Km^2 W^{-1}. This is 65% of the sensitivity to well-mixed greenhouse gases with the same coupled model; it is 81% of the sensitivity to anthropogenic aerosols [*Ming and Ramaswamy*, 2009]. The relatively low sensitivity to cloud seeding is likely partly due to seeding being highly localized in the tropics, compared to the globally uniform greenhouse gases or mid-latitude anthropogenic aerosols, as the tropics is generally less sensitive than higher latitudes partly owing to the absence of surface albedo feedback.

[15] The T response varies significantly among the individual region runs and does not scale linearly with global-mean RFP for each run (Table 1). SP is the most potent at reducing the global-mean T, while SA has an almost negligible effect, as also occurs in J09. This is borne out in their respective climate sensitivities (Table 1).

[16] Due to seeding in the SP region, the equatorial Pacific cools more in the east than in the west in the ALL (Figure 1b) and SP simulations (Figure S1 in the auxiliary material), enhancing the climatological equatorial SST gradient.[1] This strengthens the Walker circulation: over the equatorial Pacific, annual-mean 300-hPa westerly winds, near-surface easterlies, ascent in the west, and descent in the east all increase (not shown). Thus, seeding shifts the tropical Pacific to a La Niña-like state. The strengthened Walker circulation is consistent both with this La Niña-like response and with the decrease in global-mean T, which tends to enhance the strength of the tropical overturning circulation based on a thermodynamic scaling argument [*Held and Soden*, 2006; *Ming et al.*, 2010]. In contrast, the climate responses in the NP and SA simulations do not appear La-Niña-like (Figures S1b and S1f). However, little can be said about the effects of seeding in NP and SA on the equatorial Pacific SST gradient, as much of the T change for the equatorial Pacific is not statistically significant in these runs (Figures S1a and S1e).

[17] As previously noted, much of the North Pacific warms in ALL. Adjacent over northwestern Canada sits a region of exceptional cooling (Figure 1b). This T dipole is co-located with a dipole in 500-hPa geopotential heights (not shown), with heights anomalously high in the North Pacific and low over northwestern Canada. These dipoles also occur in SP, though of weaker magnitude (Figure S1c for T; geopotential heights not shown). These indicate the negative phase of the Pacific-North America oscillation (PNA), a large-scale climate variability mode [*Wallace and Gutzler*, 1981] that is correlated with ENSO (El Niño-Southern Oscillation) – the negative PNA phase with La Niña [*Horel and Wallace*, 1981]. Values of the PNA index as defined in *Wallace and Gutzler* [1981] for ALL and SP are -0.20 and -0.12, respectively. Thus, the seemingly spurious region of warming stems from the La Niña-like tropical condition caused by seeding the SP region. A similar T dipole occurs in the ALL simulation of J09 (Figure 3 of J09) and in both the 20% and 70% simulations in R09 (Figure 1 of R09), all three of which also feature seeding over the southeast tropical Pacific.

3.3. Changes in Precipitation

[18] The P response to cloud seeding depends simultaneously on multiple factors, including global-mean δT and changes to SST patterns in both the Pacific and Atlantic. Global-mean P change (δP) in ALL is -1.2% (-0.035 mm day^{-1}), which is relatively small, as global-mean P is tightly controlled by the atmospheric energy balance [*Allen and Ingram*, 2002]; the hydrological sensitivity (i.e., global-mean δP divided by global-mean δT) is 2.2% K^{-1}.

[19] The tropical P changes in ALL (Figure 1c) and SP (Figure S1d) closely resemble climatological P anomalies due to La Niña events. Specifically, P decreases across the central and eastern equatorial Pacific, while a dipole pattern

[1] Auxiliary materials are available in the HTML. doi:10.1029/2012GL052064.

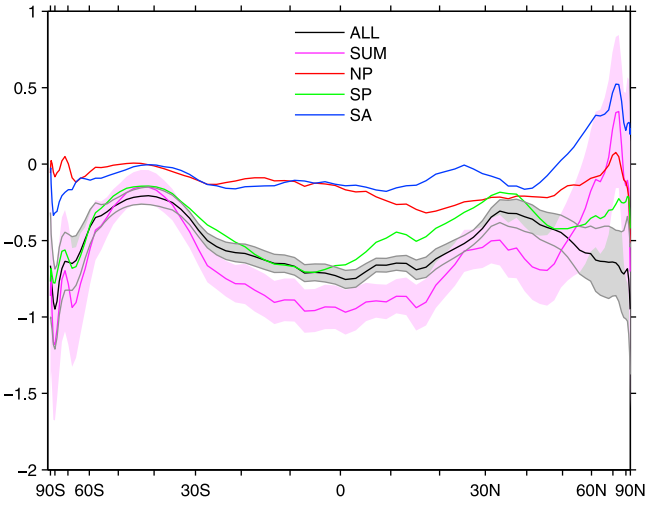

Figure 2. Zonal-mean changes in surface temperature (K) in SA, SP, NP, the linear sum of SA + SP + NP (SUM), and ALL. Shading around SUM and ALL denote 95% confidence intervals.

emerges in the western equatorial Pacific; rainfall increases strongly over the maritime continent but decreases directly northeast. We note again that, being performed with a coupled AGCM-mixed layer ocean model, these simulations do not consider possible changes in ocean dynamics. This includes the structure of the thermocline, a major factor in ENSO dynamics [*Vecchi et al.*, 2008]. This issue is best addressed with a dynamic ocean model.

[20] The P response over the Amazon Rainforest is critical to understand, given its importance ecologically and to the carbon cycle and the starkly differing responses to cloud seeding in model studies to date. Rainfall increased moderately there in R09 (Figure 3 of R09). In contrast, P decreased sharply over much of the Amazon basin in J09 (Figure 4b of J09). However, J09 used a model unique amongst current-generation GCMs in that the Amazon basin dries out almost completely in global warming simulations [*Cox et al.*, 2008; *Harris et al.*, 2008]; this model bias likely accounts for some of the P reductions.

[21] Meanwhile, most of the P response in our ALL simulation over the Amazon basin is not statistically significant (Figure 1c). (Note that the model-simulated climatological P over the Amazon does not show major biases [see *GFDL Global Atmospheric Model Development Team*, 2004, Figure 8].) Multiple opposing factors are at play. On the one hand, the La Niña-like tropical P response likely acts to increase rainfall over the Amazon [*Foley et al.*, 2002]. On the other hand, rainfall over the Amazon depends also on SST patterns in the tropical Atlantic. The tropical Atlantic cools more in the south than in the north, a pattern that has been shown to enhance subsidence over the Amazon [*Fu et al.*, 2001]. As an additional consideration, the global-mean T decrease also acts to decrease P overall [*Allen and Ingram*, 2002].

[22] In the individual region runs of J09, only SA caused significant rainfall reduction in Amazonia. In all of our individual region runs including SA, the rainfall changes over the Amazon are statistically insignificant (Figures S1b, S1d, and S1f). One might expect Amazonian rainfall to be highly sensitive to seeding in SA, given the aforementioned role of the Atlantic meridional SST gradient. But unlike in ALL, little can be said about the role of this gradient in SA, as δT in the tropical north Atlantic is mostly statistically insignificant (Figure S1e).

3.4. Nonlinearity With Respect to the Seeding Regions

[23] The linear sum of global-mean δT for NP, SP, and SA (the SUM case) is −0.63 K, which is 19% greater than that of ALL. J09 ran analogous individual region simulations, obtaining similar results, including the relative strength (weakness) of SP (SA) in reducing global-mean T and a similar degree of nonlinearity in global-mean δT in their ALL vs. SUM experiments.

[24] Analyzing zonal-mean T changes sheds additional light on the nonlinearity (Figure 2). All three individual region runs diverge substantially from ALL in the northern high latitudes, adding up to a temperature spike in SUM near 70°N. As a result, SUM is warmer than ALL north of 50°N (unlike at low latitudes), suggesting that cooling is somehow enhanced in the northern high latitudes in ALL compared to SUM. Surface albedo feedback, often invoked as an important nonlinear phenomenon near the poles, does not play a major role in this nonlinearity, as fractional change in global-mean surface albedo in SUM and ALL are nearly the same (0.7% and 0.8% respectively). In contrast, cooling is apparently weakened in the low latitudes when multiple regions are seeded together. This behavior is still under investigation.

[25] The individual region simulations show that climate response depends both on the magnitude of RFP in the global-mean and its spatial distribution. In particular, the climate is over five times more sensitive to the forcing over SP than to the one over SA (Table 1). Why is this so? It has been shown that the regional anomalies in large-scale circulation caused by an external forcing are approximately proportional to the corresponding climatological values; a good example can be found in Figure 7 of *Vecchi and Soden* [2007]. Also, the bulk of the tropical circulation, which can be viewed as a superposition of the Hadley circulation in the meridional direction and the Walker circulation in the zonal direction, occurs in the Pacific. This could mean that the impact of a forcing over SP is more likely to be felt outside the seeding region through adjusting the circulation than a forcing of similar magnitude located over SA. As another possibility, global-mean T is observed to correlate strongly with the phase of ENSO on the timescale of months [*Trenberth et al.*, 2002; *Foster and Rahmstorf*, 2011]. This appears consistent with our results, in that the SST variation over the eastern equatorial Pacific (SP) can influence global-mean δT. However, one has to interpret this with caution in light of the different time scales (i.e., months vs. 20 years).

4. Discussion

[26] Both our study and J09 demonstrate that the SP region is very effective in terms of δT. Furthermore, we have shown that seeding there directly alters the equatorial Pacific SST gradient critical to ENSO dynamics. This presents a challenge for would-be geoengineers: the region in which cloud seeding would most effectively mitigate global warming is also a region in which seeding would very likely produce intense regional climate changes, both in the tropics and the mid-latitudes through teleconnections.

[27] Constraining the climate response to cloud seeding at regional scales using GCMs is complicated by model idiosyncrasies, such as the drying out of the Amazon in the model used by J09 and the lack of marine low clouds near continents in the present study. However, several features, such as the dynamical constraint in the tropics that acts to spread out the local cooling [e.g., *Sobel et al.*, 2001; *Kang et al.*, 2009], the thermodynamically-imposed scaling of both global-mean δP and tropical circulation to global-mean δT [*Allen and Ingram*, 2002; *Held and Soden*, 2006], and the sensitivity of the climate to equatorial Pacific SSTs, are well-established theoretical results that should be robust across GCMs. They therefore provide good starting points for constraining the climate response to cloud seeding.

[28] **Acknowledgments.** We thank Tim Merlis, Caroline Muller, and two anonymous reviewers for their thorough reviews of earlier drafts. S.H. was partly supported by the NOAA Ernest F. Hollings Scholarship Program.

[29] The Editor thanks the two anonymous reviewers for assisting in the evaluation of this paper.

References

Albrecht, B. A. (1989), Aerosols, cloud microphysics, and fractional cloudiness, *Science*, *245*, 1227–1230.

Allen, M. R., and W. J. Ingram (2002), Constraints on future changes in the hydrological cycle, *Nature*, *419*, 224–228.

Ban-Weiss, G. A., L. Cao, G. Bala, and K. Caldeira (2011), Dependence of climate forcing and response on the altitude of black carbon aerosols, *Clim. Dyn.*, *38*, 897–911.

Cox, P. M., P. P. Harris, C. Huntingford, R. A. Betts, M. Collins, C. D. Jones, T. E. Jupp, J. A. Marengo, and C. A. Nobre (2008), Increasing risk of Amazonian drought due to decreasing aerosol pollution, *Nature*, *453*, 212–216.

Foley, J. A., A. Botta, M. T. Coe, and M. H. Costa (2002), El Niño-Southern oscillation and the climate, ecosystems and rivers of Amazonia, *Global Biogeochem. Cycles*, *16*(4), 1132, doi:10.1029/2002GB001872.

Foster, G., and S. Rahmstorf (2011), Global temperature evolution 1979–2010, *Environ. Res. Lett.*, *6*, 044022.

Fu, R., R. E. Dickinson, M. X. chen, and H. Wang (2001), How do tropical sea surface temperatures influence the seasonal distribution of precipitation in the equatorial Amazon?, *J. Clim.*, *14*, 4003–4026.

GFDL Global Atmospheric Model Development Team (2004), The new GFDL global atmosphere and land model AM2-LM2: Evaluation with prescribed SST simulations, *J. Clim.*, *17*, 4641–4673.

Gregory, J. M., W. J. Ingram, M. A. Palmer, G. S. Jones, P. A. Stott, R. B. Thorpe, J. A. Lowe, T. C. Johns, and K. D. Williams (2004), A new method for diagnosing radiative forcing and climate sensitivity, *Geophys. Res. Lett.*, *31*, L03205, doi:10.1029/2003GL018747.

Hansen, J., et al. (2007), Climate simulations for 1880-2003 with GISS modelE, *Clim. Dyn.*, *29*, 661–696.

Harris, P. P., C. Huntingford, and P. M. Cox (2008), Amazon Basin climate under global warming: The role of sea surface temperature, *Philos. Trans. R. Soc. B.*, *363*, 1753–1759.

Haywood, J. M., L. J. Donner, A. Jones, and J.-C. Golaz (2009), Global indirect radiative forcing caused by aerosols: IPCC (2007) and beyond, in *Clouds in the Perturbed Climate System*, edited by J. Heintzenberg and R. Charlson, pp. 451–467, MIT Press, Cambridge, Mass.

Held, I. M., and B. J. Soden (2006), Robust responses of the hydrological cycle to global warming, *J. Clim.*, *19*, 5686–5699.

Horel, J. D., and J. M. Wallace (1981), Planetary scale atmospheric phenomena associated with the Southern Oscillation, *Mon. Weather Rev.*, *109*, 813–829.

Jones, A., J. Haywood, and O. Boucher (2009), Climate impacts of geoengineering marine stratocumulus clouds, *J. Geophys. Res.*, *114*, D10106, doi:10.1029/2008JD011450.

Kang, S. M., D. M. W. Frierson, and I. Held (2009), The tropical response to extratropical thermal forcing in an idealized GCM: The importance of radiative feedbacks and convective parameterization, *J. Atmos. Sci.*, *66*, 2812–2827.

Latham, J. (1990), Control of global warming?, *Nature*, *347*, 339–340.

Latham, J. (2002), Amelioration of global warming by controlled enhancement of the albedo and longevity of low-level maritime clouds, *Atmos. Sci. Lett.*, *3*, 52–58.

Latham, J., P. Rasch, C. C. Chen, L. Kettles, A. Gadian, A. Gettelman, H. Morrison, K. Bower, and T. Choularton (2008), Global temperature stabilization via controlled albedo enhancement of low-level maritime clouds, *Philos. Trans. R. Soc. A*, *366*, 3969–3987.

Lohmann, U., L. Rotstayn, T. Storelvmo, A. Jones, S. Menon, J. Quaas, A. Ekman, D. Koch, and R. Ruedy (2010), Total aerosol effect: Radiative forcing or radiative flux perturbation?, *Atmos. Chem. Phys.*, *10*, 3235–3246.

Ming, Y., and V. Ramaswamy (2009), Nonlinear climate and hydrological responses to aerosol effects, *J. Clim.*, *22*, 1329–1339.

Ming, Y., V. Ramaswamy, L. J. Donner, and V. T. J. Phillips (2006), A new parameterization of cloud droplet activation applicable to general circulation models, *J. Atmos. Sci.*, *63*, 1348–1356.

Ming, Y., V. Ramaswamy, L. J. Donner, V. T. J. Phillips, S. A. Klein, P. A. Ginoux, and L. W. Horowitz (2007), Modeling the interactions between aerosols and liquid water clouds with a self-consistent cloud scheme in a general circulation model, *J. Atmos. Sci.*, *64*, 1189–1209.

Ming, Y., V. Ramaswamy, and G. Persad (2010), Two opposing effects of absorbing aerosols on global-mean precipitation, *Geophys. Res. Lett.*, *37*, L13701, doi:10.1029/2010GL042895.

Partanen, A.-I., H. Kokkola, S. Romakkaniemi, V.-M. Kerminen, K. E. J. Lehtinen, T. Bergman, A. Arola, and H. Korhonen (2012), Direct and indirect effects of sea spray geoengineering and the role of injected particle size, *J. Geophys. Res.*, *117*, D02203, doi:10.1029/2011JD016428.

Persad, G., Y. Ming, and V. Ramaswamy (2012), Robust tropical tropospheric responses to absorbing aerosols, *J. Clim.*, *25*, 2471–2480.

Rasch, P. J., J. Latham, and C. C. Chen (2009), Geoengineering by cloud seeding: Influence on sea ice and climate system, *Environ. Res. Lett.*, *4*, 045112.

Sobel, A. H., J. Nilsson, and L. M. Polvani (2001), The weak temperature gradient approximation and balanced tropical moisture waves, *J. Atmos. Sci.*, *58*, 3650–3665.

Trenberth, K. E., J. M. Caron, D. P. Stepaniak, and S. Worley (2002), Evolution of El Niño–Southern Oscillation and global atmospheric temperatures, *J. Geophys. Res.*, *107*(D8), 4065, doi:10.1029/2000JD000298.

Twomey, S. (1977), The influence of pollution on the shortwave albedo of clouds, *J. Atmos. Sci.*, *34*, 1149–1152.

Vecchi, G. A., and B. J. Soden (2007), Global warming and the weakening of the tropical circulation, *J. Clim.*, *20*, 4316–4340.

Vecchi, G. A., A. Clement, and B. J. Soden (2008), Examining the tropical Pacific's response to global warming, *Eos Trans. AGU*, *89*(9), 81, doi:10.1029/2008EO090002.

Wallace, J. M., and D. S. Gutzler (1981), Teleconnections in the geopotential height field during the Northern Hemisphere winter, *Mon. Weather Rev.*, *109*, 784–812.